Design and Validation of a Control Algorithm for a SAE J2954-Compliant Wireless Charger to Guarantee the Operational Electrical Constraints

José Manuel González-González *[ID], Alicia Triviño-Cabrera [ID] and José Antonio Aguado [ID]

Department of Electrical Engineering, Universidad de Málaga, 29016 Málaga, Spain; atc@uma.es (A.T.-C.); jaguado@uma.es (J.A.A.)

* Correspondence: josemanuelgonzalez@uma.es; Tel.: +34-951-952548

Abstract: Wireless power transfer is foreseen as a suitable technology to provide charge without cables to electric vehicles. This technology is mainly supported by two coupled coils, whose mutual inductance is sensitive to their relative positions. Variations on this coefficient greatly impact the electrical magnitudes of the wireless charger. The aim of this paper is the design and validation of a control algorithm for an Society of Automotive Engineers (SAE) J2954-compliant wireless charger to guarantee some operational and electrical constraints. These constraints are designed to prevent some components from being damaged by excessive voltage or current. This paper also presents the details for the design and implementation of the bidirectional charger topology in which the proposed controller is incorporated. The controller is installed on the primary and on the secondary side, given that wireless communication is necessary with the other side. The input data of the controller helps it decide about the phase shift required to apply in the DC/AC converter. The experimental results demonstrate how the system regulates the output voltage of the DC/AC converter so that some electrical magnitudes do not exceed predefined thresholds. The regulation, which has been tested when coil misalignments occur, is proven to be effective.

Keywords: inductive power transfer (IPT); wireless charger; control; electric vehicle; protection

1. Introduction

The popularity of Electric Vehicles (EV) is growing by the day. Nowadays, pollution and fuel cost volatility [1] are two main concerns that are encouraging both governments and manufacturers to make a strong commitment to EVs [2,3].

Despite the evolution that electric vehicles have experienced in recent years, this transportation mode is still associated with some disadvantages that need to be overcome. One of the most relevant issues concerns their autonomy, which fundamentally depends on the technology and capacity of the batteries. However, increasing the capacity of batteries requires a long development process. For this reason, researchers and industries are seeking other alternatives that ease the use of EVs while the battery technology evolves.

One possible solution relies on wireless chargers, which provide recharge for electric vehicles without the need for wires or user intervention. Moreover, as has been demonstrated recently, this technology allows electric vehicles to be recharged while they are moving [4,5], making this solution a feasible approach to increase their autonomy.

The wireless charge is produced by means of a high frequency alternating current that flows along a coil located on the floor (named the primary coil) and which, in turn, generates a magnetic field. This magnetic flux passes through a coil (referred to as the secondary coil) situated under the vehicle. This induces a voltage in the secondary coil and this is used to charge the battery.

The design of wireless charging systems for Electric Vehicles involves the determination of multiple parameters (mainly the coils topology and the power converters) to operate under specific conditions (e.g., distance between the coils, switching frequency). Any variation from the design conditions may negatively affect the charging process and the components of the system. These failures could be severe and may require the replacement of the component.

Moreover, the charge process of an EV wireless chargers has to be performed in a very specific way [6], as shown in Figure 1. As can be observed, there are two charging processes: the first with constant current and the second with constant voltage.
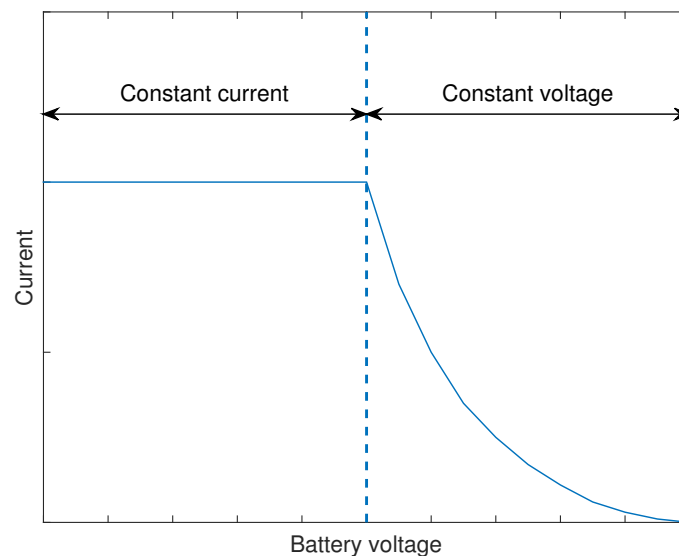

Figure 1. Processes of the charging process of a battery in an EV.

Following this charging scheme is not a trivial task because there are some time-varying conditions that affect the charge process. Thus, the power converters and the controllers become crucial as they are responsible for monitoring the voltage, the current and/or the power delivered to the battery so that they can adjust their operation by comparing the measurements with some established values. Several approaches related to the control for the EV wireless chargers have been proposed in the existing literature.

Some works focus on controlling the charging power by means of the electronics of the primary side [7]. Other proposals try to set the current either on the primary side, using a resonant inverter [8] or a DC converter [9]. The current on the secondary side can also be adjusted by regulating the inverter of the primary side [10]. Moreover, the voltage can also be controlled. For instance, Refs. [11–13] by regulating the primary voltage using different types of resonant inverters.

Despite controlling and monitoring a single variable, some of these methods are capable of working indistinctly with voltage or current to comply with the phases of the charging process. Ref. [14] presents an estimation method that prevents errors of weak communication with the capacity to control both variables. Alternatively, Ref. [15] shows a technique in which the adjustment of them is performed by a cascade buck and boost converter on the secondary side. Finally, other authors propose solutions to work with more than one variable. The goal of the control function is to achieve maximum efficiency. In this group, Ref. [16] proposes a scheme in which a primary-side-controlled charger is developed and uses a reactive power control to improve the efficiency of the system. On the other hand, Ref. [17] proposes a phase-frequency hybrid control strategy to operate at the resonant frequency.

Nevertheless, controller functions should not be limited to the discussed process as wireless chargers have to face with other potential adversities such as, for example, those derived from overpassing some electrical magnitudes. Some components are sensitive to overvoltages or overcurrents, which may cause interruptions, malfunctioning or even their destruction. These errors

could also provoke an incorrect or inefficient charge process. Thus, it is important that the controller also monitors the electrical state of the most relevant components of the wireless charger and not only the battery demands. Taking into account that coils and power converters are the components that make the wireless power transfer feasible, their electrical status should be considered by the controllers. On the one hand, the material from which the loosely coupled coils are built imposes some restrictions. These coils, which are the basis for the wireless power transfer, are usually made of Litz wire because this material minimizes the skin effect [18]. It is necessary to guarantee that the current along the wire does not exceed that allowed, as it could deteriorate the cable. It is important to note that the coils will dissipate heat that may alter other adjacent systems. On the other hand, the semiconductors of the power converters are also prone to deterioration when used incorrectly so they should operate under a range of current and/or voltage defined by their fabrication process.

Thus, the role of the controller should be an extension of those already proposed ones as it should take care of the battery and other components. This functionality is even more challenging as the electrical status of the components should be ensured even for some conditions that are not those considered in the design process. This is the case of the coil misalignment, which withstands those situations in which the relative distance between the structures of the coils differs from the one assumed in the design. As a consequence, the mutual inductance coefficient varies and the electrical magnitudes on the primary and/or secondary side are altered in comparison with the nominal ones.

From a theoretical study about the electrical consequences of the coil misalignments, this paper designs and implements a controller capable of adjusting the power transfer not only because of the requirements of the storage system, but also due to the technical constraints imposed by other components of the charger. A preliminary paper about this controller was presented in [19], but it omits the implementation concerns and the results in a real prototype.

The remainder of the paper is structured as follows. Section 2 defines the topology of the wireless charger to which we have applied the new controller. Section 3 studies the behavior of the system with different situations of coil misalignments in order to determine the most critical electrical parameter in the circuit. Section 4 presents the control technique that will be implemented in the physical controller. Section 5 shows the different components used in the laboratory and the evaluation of the proposal. Finally, Section 6 presents the main conclusions of our work.

2. Wireless Charger Topology

Wireless chargers for EVs are based on the Inductive Power Transfer (IPT) technology, which transfers the power through an air cored transformer. There is a reasonably large air gap between the primary coil, placed on the floor, and the secondary coil, located in the car. The coils counts on reactive structures known as compensation systems to operate under resonant conditions, which improve the power transfer. The magnetic field intensity and, in turn, the transferred power depend on the frequency of the current traversing the primary coil. Consequently, this technology relies on high frequency current to increase the charging power while maintaining the same primary voltage.

There are different proposals to generate this high frequency current on the primary side. The most popular solution is the full bridge inverter [8–10] due to its simplicity and its reliability. However, there are other options that lead to an improved performance at the expense of a greater complexity, such as, for example, multi-level inverters [13] or single-ended quasi-resonant converters [12]. For our design, we have opted for the full-bridge topology as it satisfies the power requirements easily. It is composed of four semiconductors (Q1, Q2, Q3 and Q4) working as switches. The reverse diodes are included to allow the current flow to the positive borne of the direct current (DC) source. In our case, the load corresponds to the coupled coils, the compensation topologies, the rectifier and the battery. Inverters require a DC source as its input. Thus, we have to use a rectifier connected to an alternating current (AC) source in the inverter input.

The generated alternating current flows through the primary coil, creating a magnetic field that mainly depends on the coil structures. As explained before, the intensity of the magnetic field

directly depends on the current and on its frequency. Between the inverter and the primary coil, a compensation system has been introduced to enable the operation under resonant conditions. For the physical implementation of this project, a series–series compensation topology has been selected due to its lower sensitivity to misalignment [20].

The magnetic field created by the primary coil passes through the secondary coil and induces an alternating voltage in it. When connected to the battery, there is an induced current. Finally, this current is converted to DC Current, which is appropriate for the battery. The conversion is performed by a rectifier, which usually is a full bridge rectifier composed of four diodes.

A similar topology can be used for bidirectional chargers or Vehicle to Grid (V2G) systems. In this case, when the system is discharging the battery and injecting power into the grid, the components are performing different functions. The secondary converter works as an inverter instead of working as a rectifier, while the primary converter works as a rectifier. Thus, bidirectional chargers require bidirectional power converters so that they can work as inverters or rectifiers depending on the direction of the power flow.

The control system is designed based on the bidirectional wireless charger topology presented in Figure 2. Nevertheless, the proposal could be extended to other schemes, for example when they include other components such as a Power Factor Corrector systems [21].
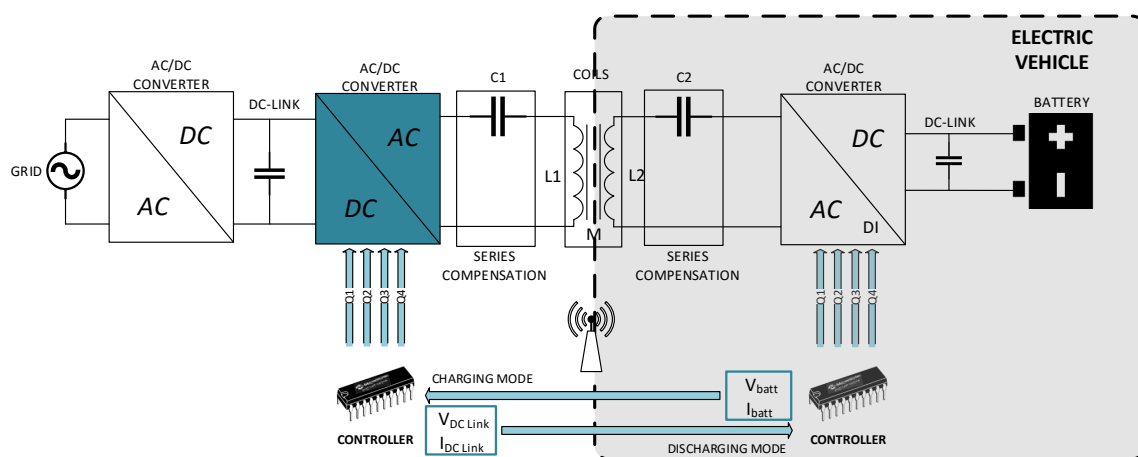

Figure 2. Topology adopted for the developed controller. This scheme is an adaptation of [19] for a bi-directional charger.

In addition to the mentioned structures, the systems include a wireless communication module so that the primary and the secondary side of the wireless charger can exchange information for the control. The control is executed in controllers that act on the switching devices of the power converters.

3. Effects of Coil Misalignments

For efficient charging, wireless EV chargers require primary and secondary coils alignment. This usually requires extra attention and time when parking.

Under realistic circumstances, the centers of the primary and secondary coils may be displaced a certain distance. This is the case of the horizontal misalignment, *xm*, as represented in Figure 3a. Horizontal misalignment could occur in both plane axes. The two coils could also be separated a certain distance (*gap*) greater/lower than the one considered in the design process (*gd*). When this happens, there is a vertical misalignment such as that shown in Figure 3b. It is usually caused by road conditions and vehicle weight. Finally, horizontal and vertical misalignment could both be present as shown in Figure 3c.
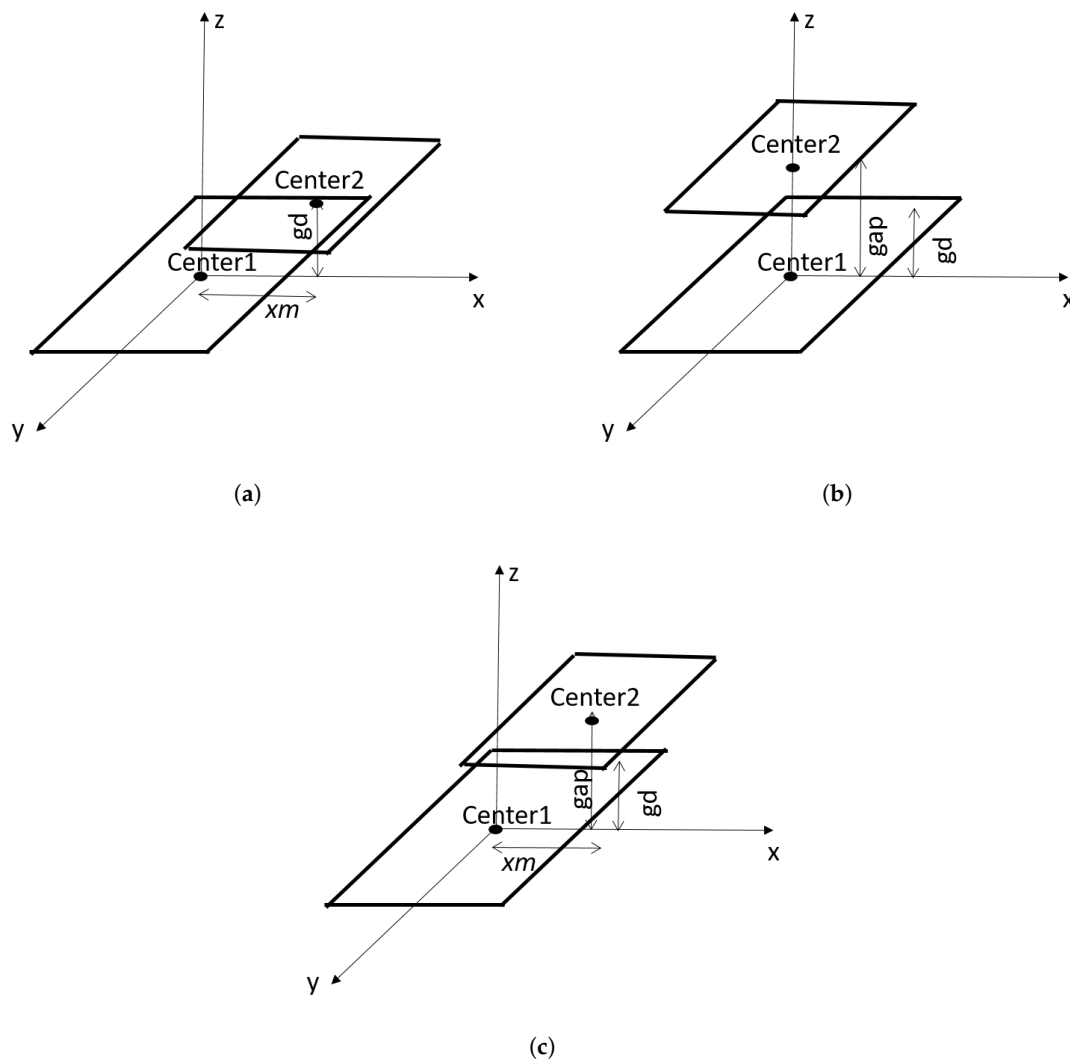
Figure 3. Types of coil misalignments. (**a**) horizontal misalignment with a *xm* displacement; (**b**) vertical misalignment with a new *gap*; and (**c**) horizontal and vertical misalignment simultaneously.

Coil misalignment impacts on magnetic and electrical magnitudes of the circuit. Specifically, coil misalignment alters the magnetic flux density traversing the secondary coil. This is modeled by the mutual inductance coefficient. The impedance reflected from the secondary side to the primary side depends on this parameter. As a consequence, variations in the mutual inductance coefficient implies changes in the voltages and currents in the system, included the primary side.

Next, we present a theoretical analysis of the equivalent circuit of a wireless charger. The equivalent circuit of an Inductively Coupled Power Transfer (ICPT) system with series–series compensation is presented in Figure 4.
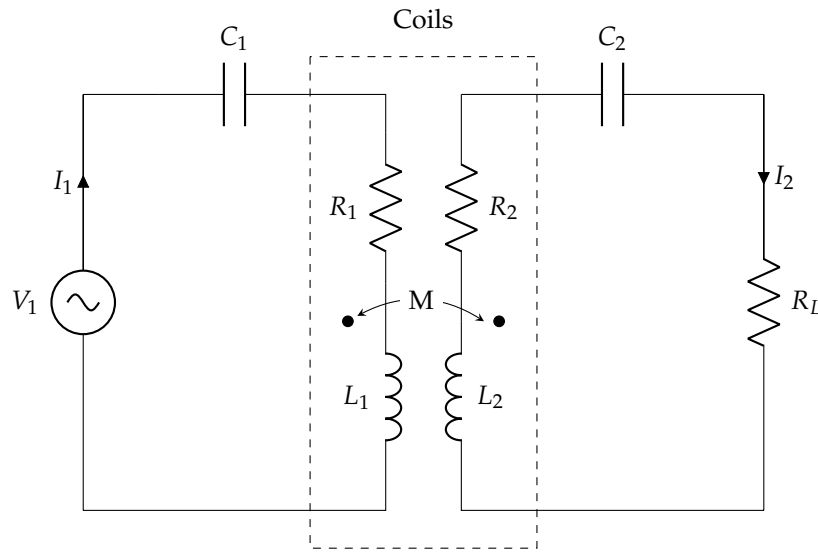
Figure 4. ICPT equivalent circuit with series–series compensation.

In this figure, L_1, L_2, R_1 and R_2 indicate the self-inductance and the resistance of primary and secondary coils, respectively. The capacitances of the compensation system of the primary and secondary side are C_1 and C_2, respectively. The currents of the primary and secondary coils are $\vec{I_1}$ and $\vec{I_2}$, respectively. The parameter M is the mutual inductance.

This compensation topology is better suited for the implementation of a control system in a bidirectional wireless charger. The capacitors are computed to force the system to operate under resonant conditions. Thus:

$$C_1 = \frac{1}{\omega^2 L_1}, \tag{1}$$

$$C_2 = \frac{1}{\omega^2 L_2}, \tag{2}$$

where ω is the frequency of the current. The parasitic capacitances of the coils are not considered in this computation. As stated in [22], an accurate model for Litz-wire rectangular coils is exclusively composed of an internal resistance and their inductance when the operating frequency is below 600 kHz.

In this equivalent circuit, R_L represents the equivalent resistance of the battery considering the effects of a rectifier.

This circuit can be analyzed using Kirchhoff's second law, which results in the following equations:

$$\vec{V_1} = [R_1 + j(L_1\omega - \frac{1}{C_1\omega})]\vec{I_1} - j\omega M \vec{I_2}, \tag{3}$$

$$0 = [(R_2 + R_L) + j(L_2\omega - \frac{1}{C_2\omega})]\vec{I_2} - j\omega M \vec{I_1}, \tag{4}$$

where $\vec{V_1}$ is the voltage at the output of the DC/AC converter. When the output of the inverter is not sinusoidal, we can work with the first harmonic approximation to derive the magnitude of $\vec{V_1}$.

The compensation systems have been designed to allow the charger to operate at resonance. Under this assumption and with Equation (4), the relation between the primary and the secondary current is shown in Equation (5):

$$\left|\frac{I_1}{I_2}\right| = \frac{R_2 + R_L}{\omega M}. \tag{5}$$

As this equation states, the relation between the primary and the secondary current is directly affected by the value of M. This implies that the relationship between the active power at the load and the one provided by the inverter is:

$$\eta = \frac{R_L}{(R_L + R_2)\left(1 + \frac{R_1(R_2+R_L)}{\omega^2 M^2}\right)} = \frac{R_L}{R_L + R_2 + R_1\left(\frac{I_1}{I_2}\right)^2}. \tag{6}$$

Consequently, η represents the efficiency of the wireless charger in the simplified model of the wireless charger in Figure 4. Efficiency is commonly studied in this type of simplified model of the charger in previous research works [23]. However, the real efficiency of the whole system should include the losses of the power converters. The work in [24] demonstrates that the inclusion of the losses of these power converters does not noticeably impact the efficiency, so Equation (6) is a suitable approach to estimate the efficiency of the system. This equation is only valid under resonant conditions and, therefore, it should be considered as the upper limit of the efficiency for a real prototype. It is worth noticing that the efficiency does not depend on the primary or secondary current but on the mutual inductance and on other constant parameters.

Next, we study how the current and the efficiency vary with M for vertical, horizontal and vertical/horizontal misalignments. We will use the concept of the impedance Z_R reflected from the secondary to the primary side. By incorporating this impedance on the primary side, we only work with the mesh related to the primary side. When C_2 is computed according to Equation (2), the value of Z_R is:

$$Z_R = \frac{\omega^2 M^2}{R_L + R_2}. \tag{7}$$

As can be observed, changes in the mutual impedance lead to variations on the reflected impedance. These modifications alter the primary and the secondary current.

This analysis is performed for square coils, but it could be extended for other topologies. We have opted for this topology as rectangular coils have been proven to offer a higher tolerance to coil misalignments than circular ones. An in-depth analysis of this sensitivity is presented in [25].

Other features of the considered wireless charger are summarized in Table 1.

Table 1. Characteristics of the analyzed wireless charger.

Frequency	85 kHz
Primary coil dimensions	0.75 m $\times$ 0.75 m
Cross-sectional area of the primary coil wire	20 mm^2
Resistance of the primary coil (R_1)	195.6 mΩ
Self-inductance of the primary coil (L_1)	240.5 μH
Secondary coil dimensions	0.5 m $\times$ 0.5 m
Cross-sectional area of the secondary coil wire	20 mm^2
Resistance of the secondary coil (R_2)	143.1 mΩ
Self-inductance of the secondary coil (L_2)	230.6 μH
Distance between coils assumed in the design (gd)	0.2 m
Compensation topology	Series-Series
Capacitance of the primary side (C_1)	17.05 nF
Capacitance of the secondary side (C_2)	15.88 nF
Load resistance	24 Ω
Input voltage of the primary inverter	170 V

The size and dimensions of the elements are feasible for the implementation of the wireless charger in an EV. The considered features include the 85 kHz frequency recommended by SAE J2954 [26]. When the coils are aligned, the power transferred to the load is 1.2 kW.

3.1. Vertical Misalignment

Vertical misalignment refers to the deviation of the distance between the coils from that assumed in the design. This displacement can occur by decreasing or increasing the distance between the two coils, which results in opposing effects that must be analyzed independently.

When a decrement in the separation of both coils happens, the value of the mutual inductance increases. As a consequence, the reflected impedance also increases according to Equation (7). When this occurs, it is not necessary to take any particular precautions because the value of the primary current decreases and the secondary current is also diminished as expressed in Equation (5).

On the other hand, increasing the vertical distance between both coils leads to the opposite effect. It decreases the mutual inductance and it reduces the reflected impedance as well. As a result, the primary and the secondary current increase. Consequently, the voltage on the secondary side increases its value and, in turn, the transferred charging power is also incremented. The augmentation of the current flowing through the components of the primary side of the charger needs to be controlled to avoid malfunctions. Figure 5 shows the evolution of the current flowing through the primary side of the charger and the coil efficiency, which has been computed as in Equation (6).
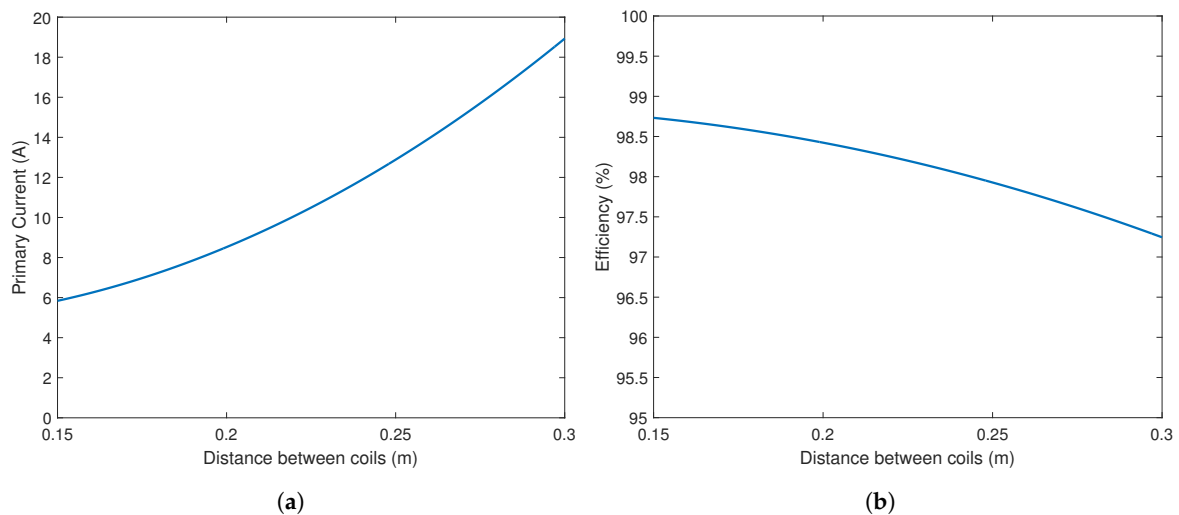

(a)   (b)

Figure 5. (**a**) primary current as a function of the distance between coils; (**b**) efficiency as a function of the distance between coils.

In order to avoid an excessive and even dangerous increase in the transferred power, the controller of the wireless charger has to act on the electronics. In particular, it decreases the voltage of the primary coil and, therefore, the primary and the secondary currents are also reduced. As a consequence, the secondary voltage and the load power are approximated to the design values.

3.2. Horizontal Misalignment

The horizontal misalignment refers to the horizontal displacement existing between the center of the primary and secondary coil, which can occur in both axes independently or simultaneously. It is the most common misalignment due to the difficulty of locating the car just above the primary coil, either in fixed or mobile situations.

This type of misalignment also affects the mutual inductance of the coils, with similar effects to the increase in the distance between coils. When a horizontal misalignment occurs, the value of the mutual inductance is reduced, increasing the transformation ratio. This results in an increment of the secondary voltage and the charging power, making it necessary for the controller to act by decreasing the transferred power. As in the previous case, the controller stabilizes the voltage and the current on the secondary side by adjusting the charging power. Figure 6 presents the evolution of the primary

current with different horizontal displacements on a single axis and the coil efficiency, which has been computed with Equation (6).
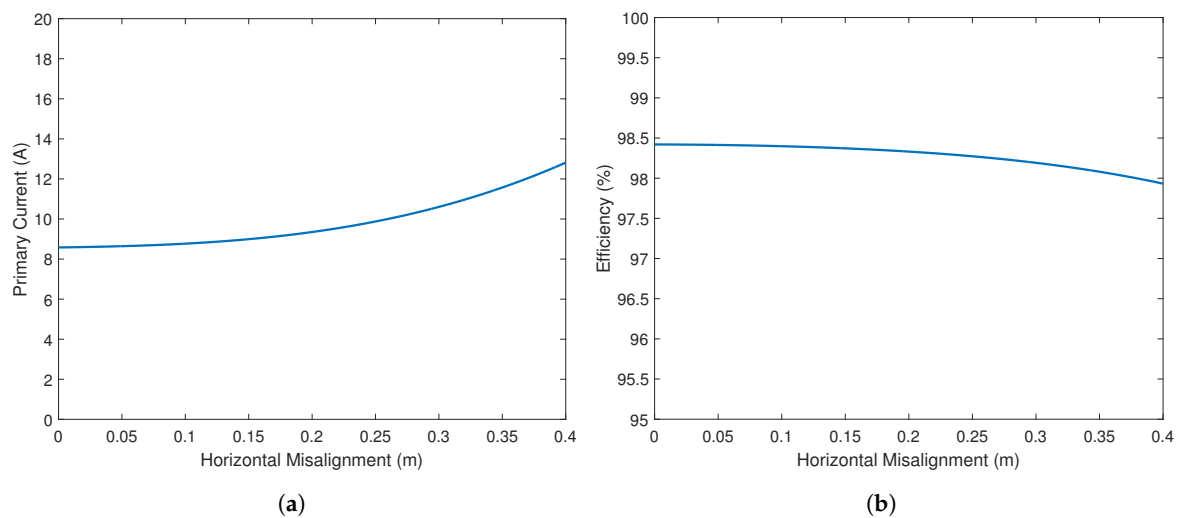

(**a**)   (**b**)

Figure 6. (**a**) primary current as a function of a horizontal misalignment; (**b**) efficiency as a function of horizontal misalignment.

As can be seen from Figure 6, the effects of horizontal misalignments are less than those of a vertical misalignment, having a very slight effect with small misalignments but growing exponentially with an increase in the displacement.

Although at first glance this increase in the value of the primary current may not be excessively large, it must be taken into account because its effects can be multiplied in combination with an vertical misalignment, which is discussed in the following subsection.

3.3. Horizontal Misalignment with 0.25 m between Coils

Finally, complementing the individualized analysis of the previous subsections, a study of the combined effects of both vertical and horizontal misalignments in both axes has been performed. In a case of actual application, it is possible to find both types of misalignment simultaneously, making the negative consequences more relevant.

In order to carry out this study, the secondary coil was located at a vertical distance of 0.25 m, which corresponds to 5 cm more than the design separation indicated in Table 1. This study is shown in Figure 7, where it is possible to observe the evolution of the primary current values with different horizontal misalignments in both axes and with a separation between coils 5 cm higher than the design.

As in the previous cases, small misalignments do not involve large increases in the values of the primary current. However, this increase in the value of the primary current occurs exponentially, exceeding 25 A with misalignments close to 40 cm.

All these analyzed cases allow the study to highlight the importance of having the primary current values under control, avoiding risks of failures and malfunctioning in the wireless charging operation. For commercial devices such as those used in our experiments, these values of current will deteriorate the semiconductors used in power converters.
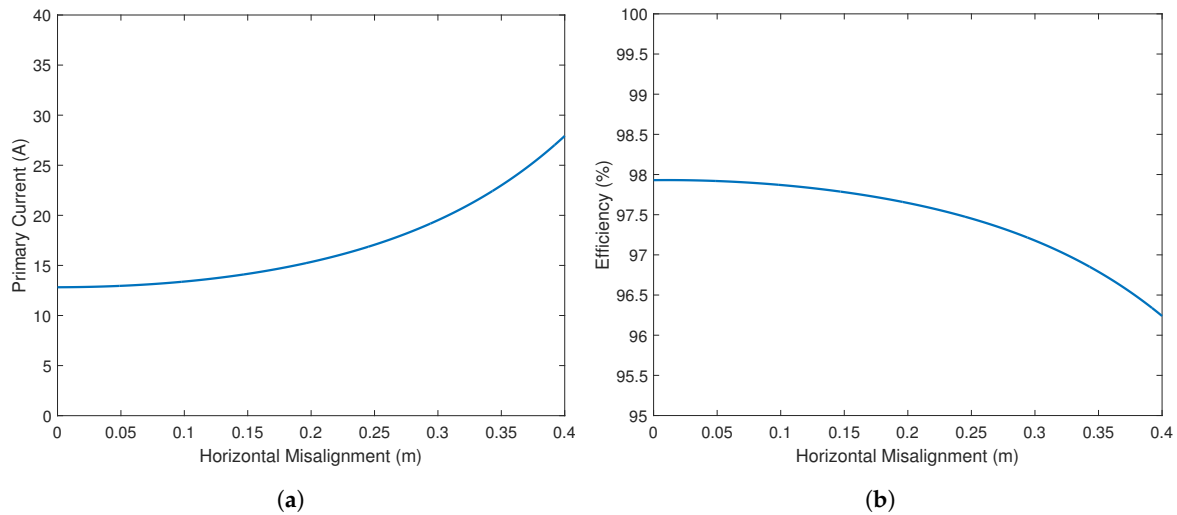
(a)   **(b)**

Figure 7. (**a**) primary current as a function of horizontal misalignment in both axes and a distance between the coils of 0.25 m; (**b**) efficiency as a function of horizontal misalignment in both axes and a distance between the coils of 0.25 m.

4. Developed Control System

The generation of the high frequency current is performed by the power converter acting as a full bridge inverter in the implemented wireless charger. One of the great difficulties of the power converter of the charger is the control system, which has to be able to regulate the charge power according to the application requirements. In our design, the functionality of the control system is even more complex as we impose additional requirements relating to the maximum current value allowable on the primary side. As explained previously, this is the first electrical magnitude that experiments a relevant increment when misalignment occurs.

The function of the control system is to activate the switching of each transistor of the converter at the right time. For this, the control strategy developed in [19] has been implemented. This strategy uses the phase-shift control technique, which is used in electrical power systems, especially in converters [27–29]. The phase-shift switching control consists of applying a delay of the transistors switching of one leg in comparison with the actuation of the switches in the other leg. In this way, it is possible to adjust the output voltage of the inverter.

Using the phase-shift technique, the first harmonic of the output voltage corresponds to:

$$V_1 = \frac{4}{\pi} V_p sin(\delta/2). \tag{8}$$

As the voltage varies with δ, the current in the primary is also affected by this parameter (please refer to Equation (3)). Consequently, the power delivered to the load is also modified according to Equation (5). However, Equation (6) indicates that this modification does not have an impact on the efficiency of the system assuming the first harmonic approximation.

Figure 8 shows the scheme of the control algorithm developed in this work.

The implemented design controls two variables: the battery power charge and the primary current, as a result of the study performed in Section 3. In order to fulfill this goal, two PI (proportional-integral) controllers have been incorporated. In our implementation, the PI_1 controller constantly performs a comparison between the measured charging power and the reference charging power, storing the error between both. The PI_2 controller allows the primary side to be protected by limiting its current. This controller monitors the current flowing through the primary side and limits it when it exceeds the maximum value allowed. The value stored by this PI is used to modify the reference charge power of the PI_1 controller, indirectly reducing the current flowing through the primary side. This error is finally

used to compute the offset between the signals of both legs (the delay), which will cause a decrement of the output voltage of the primary inverter.

Tuning the parameters of these controllers is not a trivial task, since an excessively fast action by one of them can lead to an unstable behavior of the system. Therefore, the parameters of the control system have to be carefully selected, depending on the characteristics of each charger. The effects of a bad tuning of the parameters are explained in the following section.

In our implementation, the delay of the controller is 1 s. Figure 9 shows the time that the controller takes to stabilize the output power and the primary current when an abrupt change of the position of the coil occurs. This is a limit situation, as this kind of change is not expected in a real scenario.
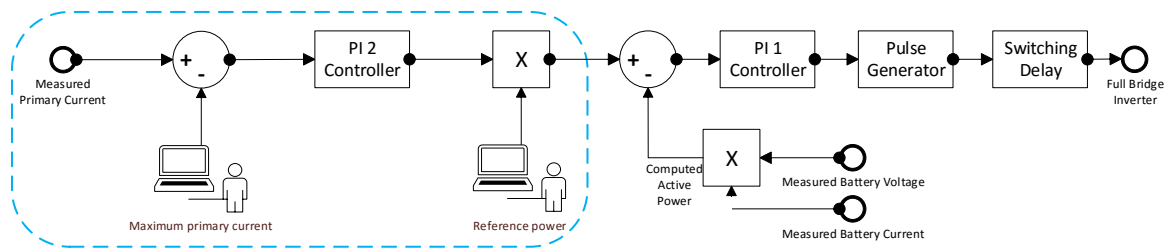

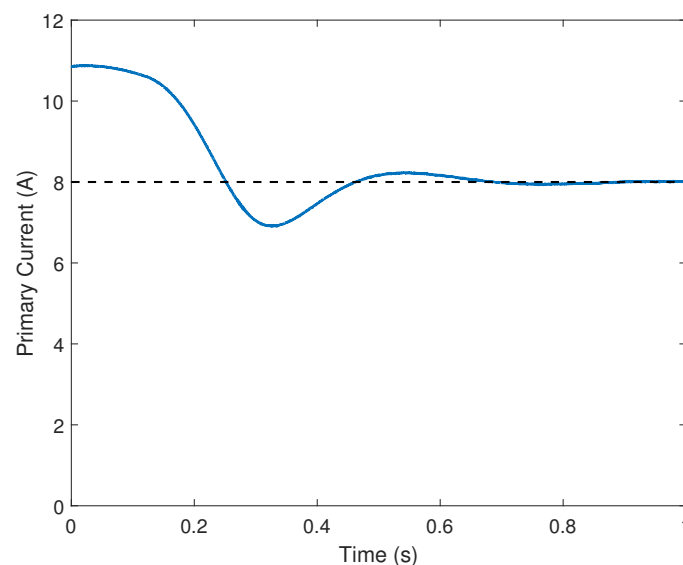**Figure 8.** Scheme of the developed control system.

Figure 9. Actuation of the implemented controller under an abrupt change of the position of the coils.

The real delay of the system should also include the effects of the communication system, which transmit the data employed as input in the controller. Specifically, the communication delay is composed of two variables: the Analog/Digital conversion of the data and the wireless transmission of this information from the secondary side to the primary side. Based on the specification of the commercial Bluetooth Low Energy module incorporated in a typical controller such as the Intel Edison (Intel, Santa Clara, CA, USA) used in our prototype, the default conversion time is 20 ms. As a result, the format of the data is a 12-bit word that needs to be transmitted through the wireless channel. Assuming that the pairing and the connection of the Bluetooth devices have been performed previously, the communication time is computed with the rate for the transmission of the data in a Bluetooth Low Energy channel. This rate is 1 Mbps. Consequently, transmitting a 16-bit word (2 bytes) implies 15.2 μs. Thus, the communication delays can be considered negligible.

Following the SAE J-2954 recommendations, the frequency of the magnetic field involved in the EV wireless charger should be 85 kHz. This implies that some electrical magnitudes also have this

frequency [30]. Consequently, the sampling and processing frequency should be adjusted to obtain valid estimations about the current and/or voltage in a component when this frequency is involved. Due to the limitations of the acquisition components of the controller, measurements of 85-kHz signals are not possible. Consequently, we have opted for the estimation of the primary current in the DC link. The other measurements are related to the battery so that they are DC and can be accurately obtained.

In addition, the transition from OFF to ON and vice versa of both transistors of the same leg can never occur simultaneously because the transistors require time to change their state once the switching signal has varied. In order to prevent short circuits in the inverter, the controller incorporates a dead time between the switching.

5. Experimental Results

The proposed system has been built in the laboratories of the Electrical Engineering Department of the University of Málaga. Figure 10 shows a picture of a part of the assembled system in which we have labeled the components. Although the results presented correspond only to the charging process, the implemented controller can work on bidirectional chargers.
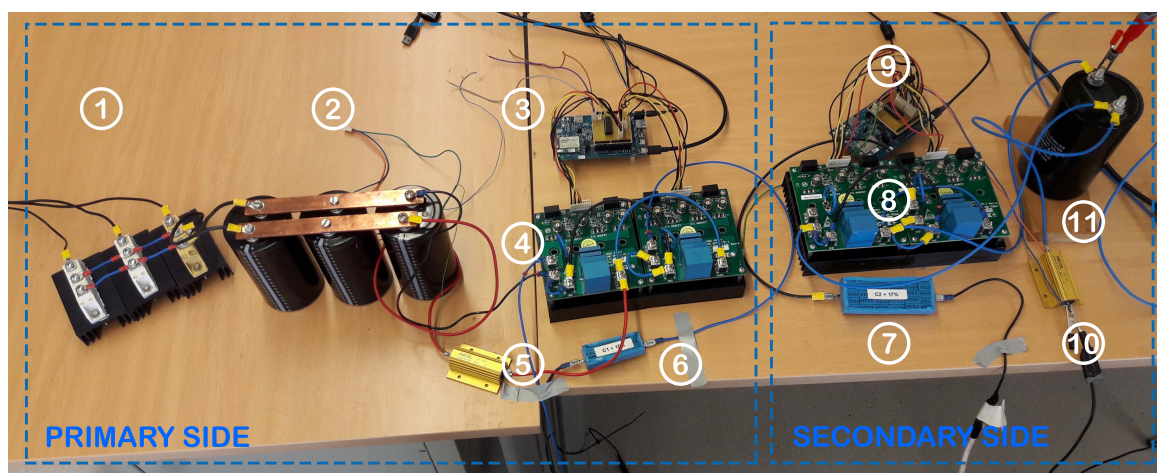

Figure 10. Picture of the assembled system in the Electrical Engineering Department of the Universidad de Málaga.

On the primary side, a three phase rectifier (number 1) is connected to the grid to generate a direct current. The DC is the input of DC/AC converter whose function is to generate a high frequency (85 kHz) alternating current. The DC/AC converter is labeled with number 4. Between both components, there are three capacitors connected in parallel (number 2) so that the equivalent capacity reduces the voltage ripple from the rectifier and, in turn, improves the performance of the inverter.

The DC/AC converter has been implemented with four Silicon Carbide (SiC) metal-oxide-semiconductor field-effect transistors (MOSFETs) following a full-bridge topology. These transistors are particularly suitable for this application as they support the required switching frequency and the current values. Moreover, they experiment a reduced amount of losses, which results in simple heat dissipation systems.

With the aim of reducing the assembly complexity, two protoboards KIT8020-CRD-8FF1217P-1 manufactured by CREE (Durham, NC, USA) have been used. Each protoboard incorporates two MOSFETs C2M0080120D and two diodes C4D20120D. The characteristics of these elements are summarized in Table 2. The MOSFETs, the diodes and the snubber circuits are shown in Figure 10. The protoboard also incorporates the electronics needed to avoid malfunctioning due to the simultaneous activation of two MOSFETs in the same leg as well the dissipation system appropriate for the heating exigencies.

Table 2. Characteristics of the C2M0080120D MOSFETs and the C4D20120D diodes.

	C2M0080120D MOSFET	
V_{DSmax}	Drain-Source Voltage	1200 V
I_D	Continuous Drain Current	36 A
$R_{DS(on)}$	Drain-Source On-State Resistance	80 mΩ
	C4D20120D Diode	
V_{RRM}	Repetitive Peak Reverse Voltage	1200 V
I_F	Continuous Forward Current	34 A
V_F	Forward Voltage	1.5 V

The DC/AC converter is controlled by a PIC microcontroller model 16F18344 [31] assembled to an Intel Edison Board (number 3 in Figure 10) [32]. The PIC provides the gate signals to the converter in accordance with the designed control. With them, the inverter generates the high frequency current incorporating the phase-shift based control. The switching delay for this control is computed by the Intel Edison Board. This value is sent to the PIC through a parallel connection. The Bluetooth communication module installed in the Intel Edison boards allows the primary controller to receive the current and the voltage values from the secondary controller. Moreover, a shunt resistor is connected to an analog input of the Intel Edison Board to estimate the primary current (number 5 in Figure 10).

Between the primary and the secondary side, there are two coils made of a Litz wire winding design as shown in Figure 11. Litz wire makes it possible to reduce the Skin effect losses in the operational frequency range [18]. Theoretically, the primary coil is located on the floor, while the secondary coil is placed in the car chassis.

Figure 11. Picture of both coils with the parameters indicated in Table 1.

Connected in series with both coils, we find the compensation systems (numbers 6 and 7 in Figure 10), formed by polypropylene film capacitors. The main advantage of this type of capacitors is their ability to support the high voltages to which they are subjected in this type of application.

The secondary side is implemented with a topology similar to that on the primary side. After the compensation system, the energy flows to the AC/DC converter (number 8), composed of the previous CREE protoboards. When the power flows from the grid to the battery, the diodes work rectifying the alternating current and converting it to direct current, which is appropriate for a battery system.

The controller of the secondary side (number 9 in Figure 10) performs a different function than that on the primary side, since in this case it is not necessary to control the AC/DC converter. The main activity of this controller is to estimate the current flowing through the battery in the DC side,

using another shunt resistor (number 10 in Figure 10). The measurement value is sent to the primary controller employing the Bluetooth communication module installed in the Intel Edison boards.

Finally, all the energy is consumed in a resistor bank with a resistance value equivalent to the battery so that the same effects of charging a battery are simulated. A capacitor (number 11) is connected in parallel to the resistors in order to improve the battery life by reducing the ripple from the rectifier. The equivalent resistance of the battery is 29.6 Ω.

The controllers were programmed in the Intel Edison board using the high-level programming language Python. In this program, we set the following electrical restrictions:

- Maximum rms current on the primary side is 8 A.
- Maximum charging power value is 1.2 kW.

These values are easily reconfigurable for other applications. We have also set the DC voltage in the primary DC/AC converter to 170 V.

With an input voltage of 170 V in the primary AC/DC converter, the system reveals the measurements presented in Figure 12 without any coil misalignment. The voltage at the output of the primary DC/AC converter has a value of 154 V, while the current flowing through the primary coil has an RMS value of 7.6 A.
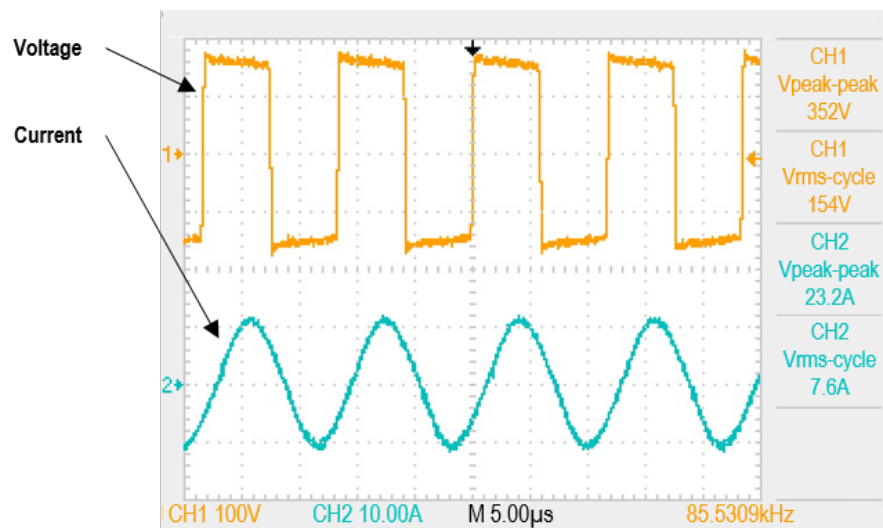

Figure 12. Voltage (channel 1) and current (channel 2) measurements at the output of the primary DC/AC converter without coil misalignments.

As expected from the analysis of Section 3, the value of the primary current increases when a coil misalignment occurs. Figure 13 presents the measurements of the system working with 0.2 m horizontal misalignment and 0.05 m vertical misalignment. Without the control system and keeping the primary input voltage constant (in yellow in Figure 13a), the primary current (in blue in Figure 13a) increases its value up to 11.36 A.

The developed control system detects that the current is expected to exceed the maximum value established in the program and begins to regulate the transmitted power using the phase shift technique. Figure 13b shows the electrical magnitudes with the intervention of the control system. In yellow, the primary output voltage is represented. This voltage measurement allows the observation of the action of the phase shift technique by forcing some dead times in the signal. In blue, the output primary current is presented. As can be noted, its value is 7.7 A. Due to the high frequency, the PIC cannot finely regulate the output voltage of the primary side and has a maximum number of regulation steps. For this reason, the value of the output current is not the maximum allowed, established in 8 A, but the regulation step immediately below 8 A.
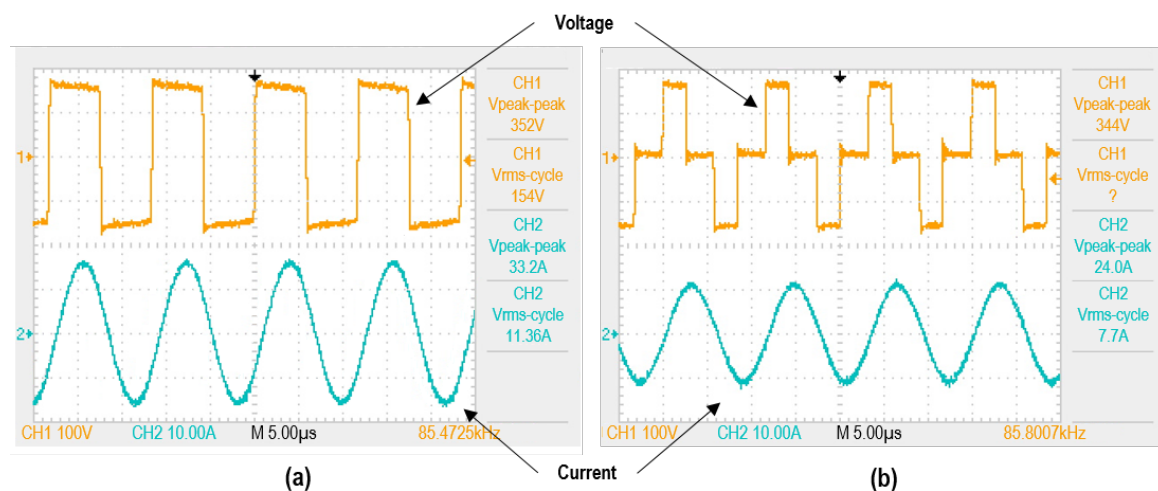
Figure 13. System working with 0.2 m horizontal misalignment and 0.05 m vertical misalignment. (**a**) primary DC voltage and current flowing through the primary coil without the proposed controller; (**b**) voltage output of the primary DC/AC converter and current flowing through the primary coil.

By computing the first harmonic of the voltage signals of the results presented in Figures 12 and 13, it is possible to derive the output power of the DC/AC converter in the primary side. The results are summarized in Table 3. The current on the secondary coil when no misalignment occurs is 9.83 A. This leads to a power delivered to the load equal to 1.15 kW. The application of the controller also impacts the power delivered to the load. The controller limits this metric to 775 W. This limitation is necessary to maintain the primary current in the specified range. However, the efficiency is slightly modified. In the case with misalignment and no control, its value is 99%. Alternatively, under the same circumstances but with the use of the proposed control technique, the efficiency is 97%. The small differences are due to the additional harmonics that the phase-shift control incorporates.

Table 3. Experimental results of the prototype.

Condition	DC/AC Output Power	Power Delivered to the Load	Efficiency
No misalignment	1.17 kW	1.15 kW	98%
Coil misalignment and no control	1.7 kW	1.69 kW	99%
Coil misalignment and control	790 W	775 W	97%

6. Conclusions

The design and implementation of a control algorithm for a wireless charger for an EV. The three main contributions of the paper are as follows: (i) the controller is adapted for a bidirectional system; (ii) the system works at 85 kHz as recommended by SAE J2954 and (iii) the controller alters the system operation in order to guarantee that the whole system works under safe conditions. The controllers, which are installed on the primary and secondary side to allow the two-directional power flow, restrict the input power based on a phase-shift control. Particularly, under coil misalignments, the primary current is the electrical magnitude that suffers from more noticeable increments. Consequently, this is one of the magnitudes that the controller restricts.

The proposed control is based on the advantage of a wireless data exchange between primary and secondary coils. Battery power charge and primary current are selected as the input variables of the control system.

It has been shown that the system correctly regulates the transmitted power to the established values under coil misalignments, preventing the charger from operating outside its limits.

Test results are described for the charging phase. We observed that the value of the primary current increases when a coil misalignment occurs but is maintained under its defined limits with the phase shift technique.

Author Contributions: The research problem addressed by the paper was identified by the three authors. The tree authors proposed the methodology and José Manuel González-González conducted the simulation study and implementation of the prototype. The results were reviewed and analysed by the three authors.

Conflicts of Interest: The authors declare no conflict of interest.

References

1. U.S. Energy Information Administration. *Annual Energy Outlook 2017 with Projections to 2050*; Technical Report; U.S. Energy Information Administration: Washington, DC, USA, 2017.
2. Holtsmark, B.; Skonhoft, A. The Norwegian support and subsidy policy of electric cars. Should it be adopted by other countries? *Environ. Sci. Policy* **2014**, *42*, 160–168.
3. Comodi, G.; Caresana, F.; Salvi, D.; Pelagalli, L.; Lorenzetti, M. Local promotion of electric mobility in cities: Guidelines and real application case in Italy. *Energy* **2016**, *95*, 494–503.
4. Miller, J.M.; Onar, O.C.; White, C.; Campbell, S.; Coomer, C.; Seiber, L.; Sepe, R.; Steyerl, A. Demonstrating Dynamic Wireless Charging of an Electric Vehicle: The Benefit of Electrochemical Capacitor Smoothing. *IEEE Power Electron. Mag.* **2014**, *1*, 12–24.
5. Maglaras, L.A.; Jiang, J.; Maglaras, A.; Topalis, F.V.; Moschoyiannis, S. Dynamic wireless charging of electric vehicles on the move with Mobile Energy Disseminators. *Int. J. Adv. Comput. Sci. Appl.* **2015**, *6*, 239–251.
6. Chen, J.-J.; Yang, F.-C.; Lai, C.-C.; Hwang, Y.-S.; Lee, R.-G. A High-Efficiency Multimode Li–Ion Battery Charger With Variable Current Source and Controlling Previous-Stage Supply Voltage. *IEEE Trans. Ind. Electron.* **2009**, *56*, 2469–2478.
7. Jiang, W.; Xu, S.; Li, N.; Lin, Z.; Williams, B.W. Wireless Power Charger for Light Electric Vehicles. In Proceedings of the 2015 IEEE 11th International Conference on Power Electronics and Drive Systems, Sydney, Australia, 9–12 June 2015; pp. 562–566.
8. Egan, M.G.; O'Sullivan, D.L.; Hayes, J.G.; Willers, M.J.; Henze, C.P. Power-Factor-Corrected Single-Stage Inductive Charger for Electric Vehicle Batteries. *IEEE Trans. Ind. Electron.* **2007**, *54*, 1217–1226.
9. Deng, J.; Lu, F.; Li, S.; Nguyen, T.D.; Mi, C. Development of a high efficiency primary side controlled 7 kW wireless power charger. In Proceedings of the 2014 IEEE International Electric Vehicle Conference (IEVC), Florence, Italy, 17–19 December 2014; pp. 1–6.
10. Lee, J.Y.; Han, B.M. A Bidirectional Wireless Power Transfer EV Charger Using Self-Resonant PWM. *IEEE Trans. Power Electron.* **2015**, *30*, 1784–1787.
11. Deng, Q.; Liu, J.; Czarkowski, D.; Bojarski, M.; Asa, E.; de Leon, F. Design of a wireless charging system with a phase-controlled inverter under varying parameters. *IET Power Electron.* **2016**, *9*, 2461–2470.
12. Iga, Y.; Omori, H.; Morizane, T.; Kimura, N.; Nakamura, Y.; Nakaoka, M. New IPT-wireless EV charger using single-ended quasi-resonant converter with power factor correction. In Proceedings of the 2012 International Conference on Renewable Energy Research and Applications (ICRERA), Nagasaki, Japan, 11–14 November 2012; pp. 1–6.
13. Asa, E.; Colak, K.; Bojarski, M.; Czarkowski, D. A novel multi-level phase-controlled resonant inverter with common mode capacitor for wireless EV chargers. In Proceedings of the 2015 IEEE Transportation Electrification Conference and Expo (ITEC), Metro Detroit, MI, USA, 14–17 June 2015; pp. 1–6.
14. Liu, F.; Chen, K.; Zhao, Z.; Li, K.; Yuan, L. Transmitter-Side Control of Both the CC and CV Modes for the Wireless EV Charging System with the Weak Communication. *IEEE J. Emerg. Sel. Top. Power Electron.* **2017**, doi:10.1109/JESTPE.2017.2759581 .
15. Colak, K.; Bojarski, M.; Asa, E.; Czarkowski, D. A constant resistance analysis and control of cascaded buck and boost converter for wireless EV chargers. In Proceedings of the 2015 IEEE Applied Power Electronics Conference and Exposition (APEC), Charlotte, NC, USA, 15–19 March 2015; pp. 3157–3161.
16. Miller, J.M.; Onar, O.C.; Chinthavali, M. Primary-Side Power Flow Control of Wireless Power Transfer for Electric Vehicle Charging. *IEEE J. Emerg. Sel. Top. Power Electron.* **2015**, *3*, 147–162.

17. Bojarski, M.; Asa, E.; Colak, K.; Czarkowski, D. A 25 kW industrial prototype wireless electric vehicle charger. In Proceedings of the 2016 IEEE Applied Power Electronics Conference and Exposition (APEC), Long Beach, CA, USA, 20–24 March 2016; pp. 1756–1761.

18. Deng, Q.; Liu, J.; Czarkowski, D.; Kazimierczuk, M.K.; Bojarski, M.; Zhou, H.; Hu, W. Frequency-Dependent Resistance of Litz-Wire Square Solenoid Coils and Quality Factor Optimization for Wireless Power Transfer. *IEEE Trans. Ind. Electron.* **2016**, *63*, 2825–2837.

19. Gonzalez-Gonzalez, J.M.; Trivino-Cabrera, A.; Aguado, J.A. Control algorithm for wireless EV charger considering operational constraints of electrical components. In Proceedings of the 2017 11th IEEE International Conference on Compatibility, Power Electronics and Power Engineering (CPE-POWERENG), Cadiz, Spain, 4–6 April 2017; pp. 211–216.

20. Aditya, K.; Williamson, S.S. Comparative study of Series-Series and Series-Parallel compensation topologies for electric vehicle charging. In Proceedings of the 2014 IEEE 23rd International Symposium on Industrial Electronics (ISIE), Istambul, Turkey, 1–4 June 2014; pp. 426–430.

21. González-González, J.M.; Cabrera, D.F.; Cabrera, A.T.; Aguado, J.A. Power Factor Corrector Design applied to an 85-kHz Wireless Charger. In Proceedings of the International Conference on Renewable Energies and Power Quality (ICREPQ'16), Madrid, Spain, 4–6 May 2016; pp. 521–525.

22. Otomo, Y.; Sato, Y.; Fujita, S.; Igarashi, H. Synthesis of Equivalent Circuit of Wireless Power Transfer Device Using Homogenization-Based FEM. *IEEE Trans. Magn.* **2017**, doi:10.1109/TMAG.2017.2749968 .

23. Tran, D.H.; Vu, V.B.; Choi, W. Design of a High-Efficiency Wireless Power Transfer System With Intermediate Coils for the On-Board Chargers of Electric Vehicles. *IEEE Trans. Power Electron.* **2018**, *33*, 175–187.

24. Deng, Q.; Liu, J.; Czarkowski, D.; Hu, W.; Zhou, H. An Inductive Power Transfer System Supplied by a Multiphase Parallel Inverter. *IEEE Trans. Ind. Electron.* **2017**, *64*, 7039–7048.

25. Fotopoulou, K.; Flynn, B.W. Wireless Power Transfer in Loosely Coupled Links: Coil Misalignment Model. *IEEE Trans. Magn.* **2011**, *47*, 416–430.

26. SAE International. *SAE International Approves TIR J2954 for PH/EV Wireless Charging*; SAE International: Warrendale, PA, USA, 2016.

27. Liu, X.; Wang, T.; Yang, X.; Jin, N.; Tang, H. Analysis and Design of a Wireless Power Transfer System with Dual Active Bridges. *Energies* **2017**, *10*, 1588, doi:10.3390/en10101588.

28. Berger, A.; Agostinelli, M.; Vesti, S.; Oliver, J.A.; Cobos, J.A.; Huemer, M. A Wireless Charging System Applying Phase-Shift and Amplitude Control to Maximize Efficiency and Extractable Power. *IEEE Trans. Power Electron.* **2015**, *30*, 6338–6348.

29. Chen, B.-Y.; Lai, Y.-S. Switching Control Technique of Phase-Shift-Controlled Full-Bridge Converter to Improve Efficiency Under Light-Load and Standby Conditions Without Additional Auxiliary Components. *IEEE Trans. Power Electron.* **2010**, *25*, 1001–1012.

30. Triviño-Cabrera, A.; Aguado, J.; González, J.M. Analytical characterisation of magnetic field generated by ICPT wireless charger. *Electron. Lett.* **2017**, *53*, 871–873.

31. Microchip. *PIC16(L)F18324/18344 Datasheet*; Microchip Technology: Chandler, AZ, USA, 2017.

32. Intel. *Intel Edison Compute Module Hardware Guide*; Intel: Santa Clara, CA, USA, 2016.